www.pss-b.com

MOVPE-Growth of InGaSb/AlP/GaP(001) Quantum Dots for Nanoscale Memory Applications

Elisa M. Sala, Ismail F. Arikan, Leo Bonato, Frank Bertram, Peter Veit, Jürgen Christen, André Strittmatter, and Dieter Bimberg*

The structural and optical properties of InGaSb/GaP(001) type-II quantum dots (QDs) grown by metalorganic vapor phase epitaxy (MOVPE) are studied. Growth strategies as growth interruption (GRI) after deposition of InGaSb and Sb-flush prior to QD growth are used to tune the structural and optical properties of InGaSb QDs. The Sb-flush affects the surface diffusion leading to more homogeneous QDs and to a reduction of defects. A ripening process during GRI occurs, where QD size is increased and QD-luminescence remarkably improved. InGaSb QDs are embedded in GaP n + p-diodes, employing an additional AlP barrier, and characterized electrically. A localization energy of 1.15 eV for holes in QDs is measured by using deep-level transient spectroscopy (DLTS). The use of Sb in QD growth is found to decrease the associated QD capture cross-section by one order of magnitude with respect to the one of $In_{0.5}Ga_{0.5}As/GaP$ QDs. This leads to a hole storage time of almost 1 h at room temperature, which represents to date the record value for MOVPE-grown QDs, making MOVPE of InGaSb/GaP related QDs a promising technology for QD-based nano-memories.

1. Introduction

Self-assembled quantum dots (QDs) have recently attracted great attention due to their promises as future storage units in a new type of electronic nanoscale memory, the QD-Flash.[1,2] Type-II antimony-based QDs exhibiting sole hole confinement are very suitable for this application, leading to a higher carrier localization energy and an increased carrier storage capacity for a single QD, with respect to type-I heterostructures.[3,4] Type-II QDs are therefore considered the best candidates as building

blocks for the future QD-Flash. Recently, we successfully demonstrated for the first time MOVPE growth of a new Sb-based QD-system, that is, InGaSb QDs embedded in a GaP matrix.[5] Up to now, the longest published storage time for MOVPE-grown QDs is 230 s at room temperature for $In_{0.5}Ga_{0.5}As/GaP$ QDs.[6] Holes trapped in GaSb/GaP QDs grown by MBE have shown 4 days retention time[7]; MBE is however not considered as a technology for mass production of electronic devices, and in particular memories.

The storage time τ for holes in QDs can be expressed as the inverse of the thermal emission rate e_a for holes from QDs[8]:

$$e_a = \gamma \, T^2 \sigma_\infty \exp\left(-\frac{E_a}{k_B T}\right) \tag{1}$$

where E_a is the activation energy, k_B the Boltzmann constant, T the temperature, σ_∞ the capture cross-section for $T = \infty$, and γ a constant depending only on the hole effective mass and degeneracy of hole states. The tunneling emission is negligible since the applied electric field is small and the temperature of interest is high.[9] Hence, the storage time τ depends solely on E_a (representing the energy barrier that holes need to surpass in the emission process) and on σ_∞, which measures the scattering probability of holes with the surrounding matrix. σ_∞ depends on many physical parameters, like QD geometry and QD interaction with the surroundings.[10] In previous measurements, σ_∞ has been observed to vary over six orders of magnitude.[11] From this observation follows that a reliable method for engineering the cross-section would represent a valuable tool for the extension of hole retention time in QDs. In practice, cross-section engineering is achieved by acting on the structural and electronic properties of the QDs. In this work, we report on the increase by about a factor of 14 of the hole storage time for InGaSb/GaP QDs grown via MOVPE, as compared to our former result on $In_{0.5}Ga_{0.5}As/GaP$ QDs.[6] Such improvement has been obtained by employing Sb during QD growth, which has reduced the associated QD capture cross-section, thereby leading to the highest measured hole localization energy for MOVPE-grown QDs so far. Moreover, the MOVPE growth technique enables large-scale and cost-effective production of device structures, thus being advantageous for the future fabrication on QD-based nanoscale memory devices. Here, we

Dr. E. M. Sala, Dr. I. F. Arikan, Dr. L. Bonato, Prof. D. Bimberg
Institut für Festkörperphysik
Technische Universität Berlin
Hardenbergstraße 36, 10623 Berlin, Germany
E-mail: elisa.m.sala@campus.tu-berlin.de; e.maddy87@gmail.com

Dr. F. Bertram, Dr. P. Veit, Prof. J. Christen, Prof. A. Strittmatter
Otto von Guericke Universität Magdeburg
Universitätsplatz 2, 39016 Magdeburg, Germany

Prof. D. Bimberg
Chinese-Geman Center on Green Photonics of the Chinese Academy of Sciences at CIOMP
Changchun 13033, China

also show that QD structural and optical properties can be tuned by exploiting two different strategies: 1) an Sb-flush (antimony-*soaking*) before QD deposition and 2) a growth interruption (GRI) step after QD formation. These techniques affect noticeably the structural and optical properties of QDs, thus paving the way for future studies of their impact on QD capture cross-section design and increase of retention time.

2. Sample Preparation

All samples were fabricated via MOVPE in a horizontal Aixtron 200 reactor on GaP (001) substrates. After growing a 500 nm undoped GaP buffer at 750 °C, a 5 ML-thick GaAs interlayer is deposited at 500 °C to enable the following QD formation, as already shown in our previous work.[5] For a sample batch, an antimony-flush with different durations (t_{Sb}) has been used prior to QD deposition, with a *triethyl-antimony* (TESb) input flux kept constant at 2.6 µmol min^{-1}. Thereafter InGaSb is provided to the reactor for QD formation. For a sample set, a GRI without any precursor supply for group-V stabilization has been applied after QD deposition to study the QD evolution. For structural investigations the samples are immediately cooled down after QD growth. For optical measurements, instead, QDs have been overgrown by an additional 50 nm GaP capping layer at 600 °C. For electrical characterizations via deep-level transient spectroscopy (DLTS), three dedicated samples were fabricated, as depicted in **Figure 1**: one containing InGaSb QDs ("*Only-QD*"), one with QDs and an additional AlP layer ("*QD-Barr*") and one as reference, containing only the AlP layer ("*Only-Barr*"). For the samples *Only-QD* and *QD-Barr*, an Sb-flush of 4 s has been used. The DLTS structures are in form of n^+p-diodes, grown on p-doped GaP (001) substrates (nominal p-doping $\approx 1.5\,10^{18}$ cm^{-3}). The first segment of each diode consists of ≈ 300 nm thick p-GaP, doped with carbon, by using *carbon trichloro-bromide* (CCl$_3$Br) as precursor (with an input flux of ≈ 1.1 µmol min^{-1} and V/III ratio of 13, growth temperature $T_g = 620$ °C), which results in a doping concentration of $\approx 5\,10^{[16]}$ cm^{-3}. For samples *Only-Barr* and *QD-Barr*, a ≈ 20 nm AlP layer is employed, which acts as an emission barrier for charge-carriers in the QDs ($T_g = 800$ °C) and finally overgrown with a thin GaP layer (≈ 2 nm). The AlP barrier aims to increase the localization energy of holes in the QDs and therefore their storage time. Instead, the

GaP capping is used to protect AlP from adsorbing impurities during the cooling down step following the QD growth. Thereafter, GaAs interlayer and QDs are grown and capped with 6 nm undoped GaP, $T_g = 500$ °C. They are followed by a GaP p-layer (≈ 500 nm) having a nominal doping concentration of $\approx 5\,10^{16}$ cm^{-3}, deposited at $T_g = 620$ °C. The last segment of the n^+-p-diode consists in a highly n-doped GaP layer ($\approx 5\,10^{18}$ cm^{-3}, $T_g = 620$ °C), where silicon is used as dopant.

The DLTS samples are processed via standard optical lithography and dry etching methods. Ni/Au-Ge/Au top contacts with diameters of 400 and 800 µm are thermally evaporated on the highly n-doped layer, whereas Ni/Zn/Au contacts are deposited on the back side (p-doped substrate) of the samples. After deposition, the samples are annealed at 400 °C for 3 min in a nitrogen atmosphere.[12–14]

To study the influence of a varying Sb-flush time (t_{Sb}) applied after the GaAs interlayer and before QD growth, a sample set with t_{Sb} ranging from 0 to 4 s was prepared. Although the microscopic mechanism of surface-active species as Sb in heteroepitaxial growth is still under debate, antimony is generally used as a way for controlling the formation and electronic properties of QDs[15,16–20]: it has been reported that antimony reduces the surface energy and therefore the adatom surface diffusion.[15,16,18] Sb-assisted QD-growth can therefore lead to smaller and more homogeneous QDs, thereby suppressing defect formation and increasing the QD density.[17,19]

3. Structural and Optical Characterizations

In **Figure 2** three AFM micrographs of free-standing QDs are displayed, where different t_{Sb} are applied. In (a) QDs are grown without Sb-flush: the QD areal density is $\approx 6\,10^{10}$ cm^{-2}, the diameter is (35 ± 6) nm, and the height (2.6 ± 0.5) nm. Here, the large objects (marked with circles) are attributed to plastically relaxed QDs since material accumulation is strongly enhanced. These objects have a density of $\approx 10^9$ cm^{-2} and dimensions of (53 ± 3) and (3.2 ± 0.3) nm for width and height, respectively.
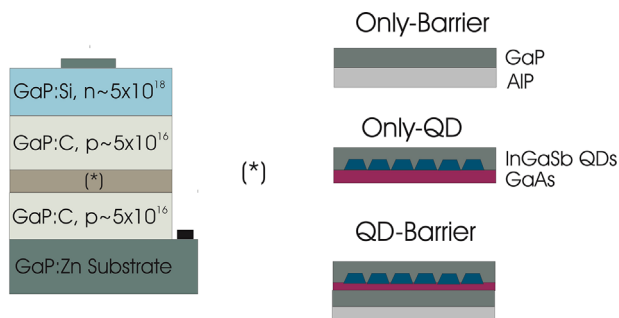

Figure 1. Design of the three DLTS structures. The asterisk indicates the different types of layer structure containing, from top right, only the AlP barrier, only QDs, or QDs + AlP.
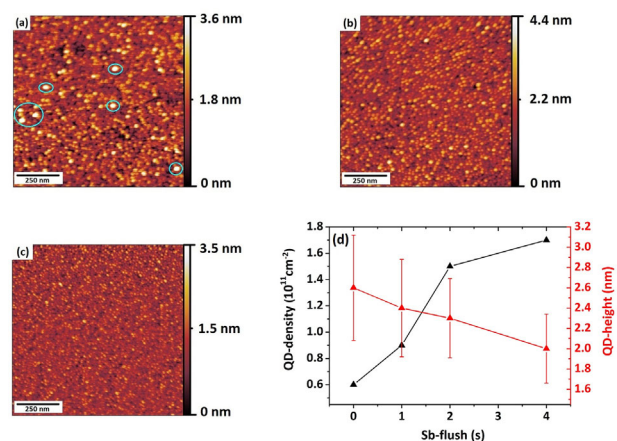

Figure 2. AFM micrographs of free-standing 0.51 ML InGaSb QDs: without (a), with 1 s (b), and 4 s (c) Sb-flush. In (d) the variation of QD-density and −height versus Sb-flush duration is shown.

Upon prolonging the Sb-flush time, the formation of these large objects is reduced: with $t_{Sb} = 1\,s$ their density is down to $\approx 10^8\,cm^{-2}$, and for $t_{Sb} \geq 2\,s$ their formation is totally suppressed. Simultaneously, QDs appear smaller and more uniform: in plot 2 (d) the QD density and height versus t_{Sb} is presented: for 4 s flush, QDs have lateral dimensions of (24 ± 3) and (2 ± 0.3) nm, with density $\approx 1.7\,10^{11}\,cm^{-2}$.

To evaluate the impact of the Sb-flush on the optical properties, a PL sample set with different t_{Sb} has been fabricated (as for the AFM-batch, 0, 2, and 4 s). In **Figure 3** their PL spectra taken at room temperature are presented: the highest PL integrated intensity can be found for $t_{Sb} = 4\,s$, which shows an improvement of $\approx 45\%$ with respect to $t_{Sb} = 0\,s$. At the same time, the FWHM of the QD-emission is slightly reduced ($\approx 5\%$) with longer t_{Sb}, as displayed in the right inset of Figure 3 and simultaneously, a blue-shift of $\approx 5\,meV$ can be detected. These observations indicate that QDs become more homogeneous with a prolonged t_{Sb} and at the same time defects are reduced, as also observed in the AFM micrographs.

In **Figure 4**a a cross-sectional STEM image (high-angle-annular-darkfield contrast) of a PL sample with QDs reveals the complete layer structure. It is composed of InGaSb QDs embedded in a structure consisting of: 1) a GaP buffer layer; 2) a $\approx 20\,nm$-thick $Al_{0.4}Ga_{0.6}P$ layer; 3) 150 nm GaP spacing; 4) 5 ML GaAs interlayer; 5) InGaSb QDs; and 5) $\approx 50\,nm$-thick GaP capping layer. The white, horizontal line indicates the position of the QD layer, while the dark broad line displays the 20 nm $Al_{0.4}Ga_{0.6}P$ layer. Simultaneously, cathodoluminescence (CL) spectroscopy was carried out in a scanning transmission electron microscope. Figure 4b shows a CL line scan recorded at a temperature of 15 K across the layer structure seen in Figure 4a. The emission around 700 nm originates from the QD growth region. Another contribution is found in the range of 2.2–2.3 eV close to the GaP energy gap where neutral donor bound exciton (D^0,X) transition in GaP exists.[21]
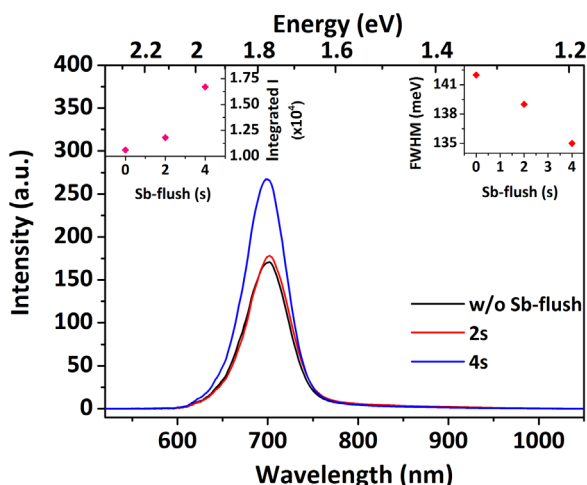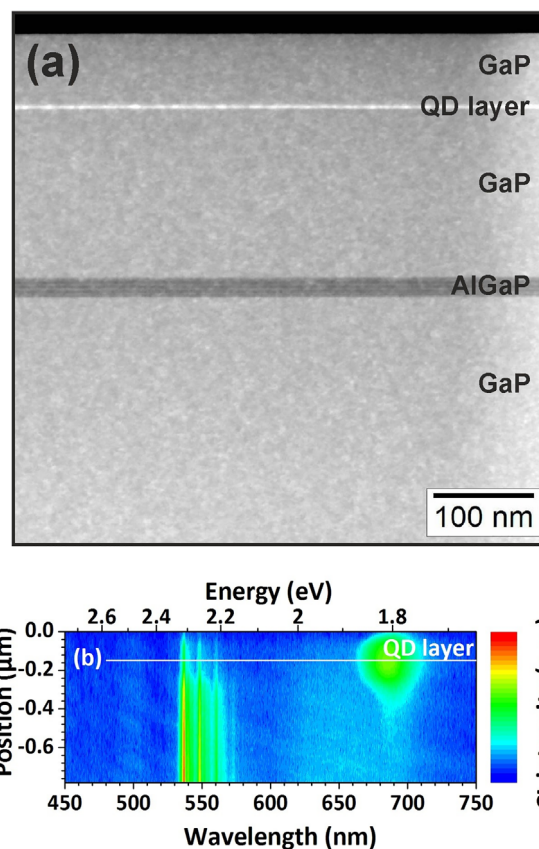

Figure 4. a) Cross-section view of the sample with buried 0.51 ML InGaSb QDs in HAADF contrast showing the QD layer as white, horizontal line 50 nm below the top surface. The dark broad line 20 nm thick is the AlGaP layer. b) Cathodoluminescence spectral linescan at 15 K: the white dotted line marks the position of the quantum dots. The emission around 1.85 eV originates from the InGaSb/GaAs/GaP QD region, whereas the emission around 2.5 eV belongs to the GaP excitonic emission (including phonon replica).
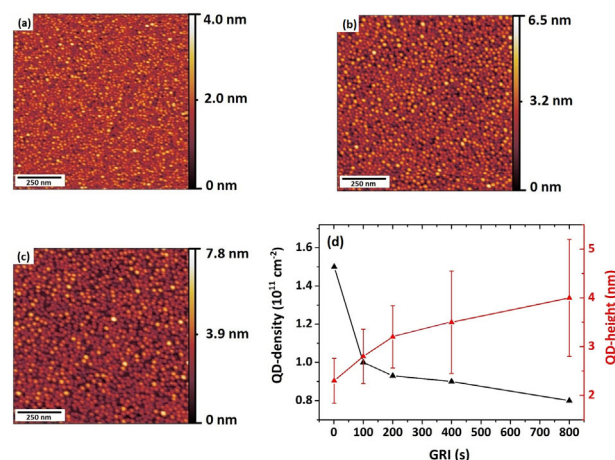

Figure 3. PL spectra at room temperature of buried 0.51 ML InGaSb QDs, grown with different t_{Sb}. In inset on the right the FWHM of the QD-emission is plotted versus t_{Sb}. In inset on the left the total integrated PL-intensity versus t_{Sb} is displayed.

Figure 5. AFM micrographs of free-standing 0.51 ML InGaSb QDs with different GRI durations: (a) 1 s, (b) 200 s, and (c) 800 s. In (d) the variation of QD-density and -height versus GRI is depicted. 2 s Sb-flush has been used for all samples.

ADVANCED
SCIENCE NEWS
www.advancedsciencenews.com

physica
status
solidi b

www.pss-b.com

Another way to control the structural and optical properties of QDs is to employ a GRI step after the QD deposition. Indeed, a GRI applied immediately after QD formation promotes material transfer between 3D islands, thereby increasing the QD size and reducing their density (process known as QD-*ripening*).[22,23] Here, we apply GRI times ranging from 1 to 800 s after QD deposition at the same growth temperature, without any supplemental precursor supply. In **Figure 5** AFM micrographs of InGaSb QDs with different GRIs are presented. For 1s GRI (Figure 5a), QDs have lateral dimensions of (28 ± 4) nm and height of (2.3 ± 0.4) nm at a density of $\approx 1.5\,10^{11}\,cm^{-2}$. As shown in the plot in Figure 5d, with longer GRI the QD density decreases, while QDs grow bigger in size: after 400 s, the islands have diameters of (31 ± 7) nm and heights of (3.5 ± 1) nm. For 800 s, lateral dimensions reach (33 ± 8) nm and height (4 ± 1.2) nm with density $\approx 8\,10^{10}\,cm^{-2}$. Ripening via material transfer between the QDs is thus concluded.

In **Figure 6** PL spectra of QDs grown for different GRIs are displayed. The QD-emission is detected between 1.76 and 1.81 eV, for 1–800 s GRI. The total integrated intensity is increased by 80% for 800 s with respect to 1 s, remaining apparently stable upon further GRI increase. An extended GRI time leads to a redshift in the QD-emission (≈ 50 meV) toward longer wavelengths, which reflects the increase of the average QD-volume, as also supported by AFM investigations. For shorter GRIs an additional luminescence around 1.9–2 eV is observed, which can be ascribed to the emission caused by island formation occurring at the interface of the thin GaAs quantum well (QW).[24] In fact, according to theoretical predictions and experimental investigations reported in,[25] ML-fluctuations of a GaAs QW exhibit luminescence in the range of 1.9–2 eV. With increasing QD size (800 s GRI interruption time), the high energy luminescence quenches, while the QD luminescence intensity increases. Assuming that free holes are efficiently captured by QD hole states a reconfiguration of electron states is concluded. As in the case of InGaAs/GaP QDs,[26] strain induced
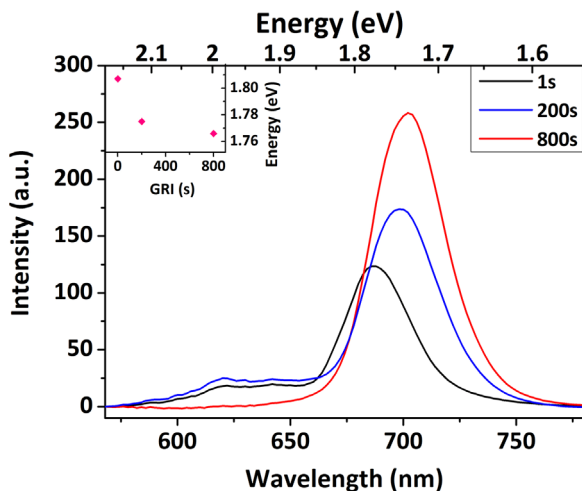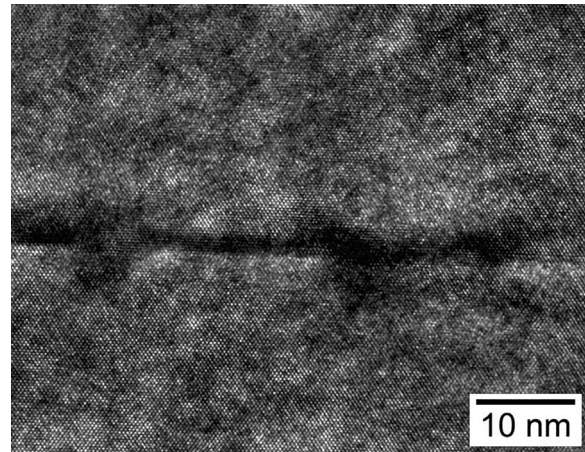

Figure 7. High resolution TEM image of 0.51 ML InGaSb QDs, 1 s GRI, capped with 6 nm GaP. The QD regions appear as dark contrast areas. The 5 ML GaAs (deposited prior to the InGaSb QDs) cannot be resolved as a continuous layer anymore.

electron states around the QD region may evolve to lower energies than the WL states with increasing QD size.

In order to get microstructural insight into material distribution, high-resolution transmission electron microscopy images were also taken from the sample investigated by CL (see Figure 4a). In **Figure 7** a high-resolution cross-section TEM image of the QD region is shown. The QDs appear as dark contrast within the GaP matrix. Interestingly, no GaAs interlayer can be identified. Apparently, a certain amount of GaAs from interlayer gets incorporated into QDs during QD formation, as also deduced from the dependence of QD morphology on interlayer thickness shown in our previous work.[5] Moreover, the energetic position of the QD-luminescence (≈ 1.75 eV) is comparable to the one of $In_{0.5}Ga_{0.5}As/GaP$ QDs.[26] From these results, we can infer that a considerable amount of As might have replaced Sb in the QDs, thus reducing the actual Sb content.

4. Electrical Characterization

The electrical characterization consists of static capacitance spectroscopy (C–V profiling) and time-resolved capacitance spectroscopy, DLTS.[27] DLTS allows for the determination of activation energy and capture cross-section. Since hole localization in the QDs reduces the capacitance of the p-n junction, C–V profiling can be used to determine the voltages at which holes are captured into and released from the QDs,[28] thereby defining the interval of interest for DLTS. In DLTS measurements, the voltage is initially set to the measurement voltage V_m, chosen such that no holes are localized in the QDs (QDs completely discharged). The voltage is then increased to the pulse voltage V_p to lower the Fermi level and fill the QDs with holes. After all energy levels of the QDs are filled, the voltage is returned to the initial value V_m, inducing hole emission. The emission process is observed via time-resolved measurement of the capacitance transient and the measurement cycle is repeated for several temperatures. The

Figure 6. PL spectra of buried 0.51 ML InGaSb QDs, 2 s Sb-flush, recorded at 40 K, grown with different GRI durations. In inset the energy shift of the QD-emission is plotted against GRI.

resulting data are analyzed using the double-boxcar method and displayed in an Arrhenius plot, from which activation energy and capture cross-section are extracted via a linear fit. The *conventional* DLTS measurement yields the average value of the activation energy over all bound states of the QDs (i.e., the *mean, ensemble* activation energy). Additionally *charge-selective* DLTS[29] is performed to determine the activation energy of the hole ground state, which is referred to as *hole localization energy*, meaning the energy difference between the hole ground state and the valence band edge of the surrounding matrix material. In charge-selective DLTS the voltages are increased in small steps in the measurement interval, so that only one of the internal levels of the QDs is involved in each measurement step: ideally, one hole per QD enters and leaves the QD in each DLTS cycle. The charge-selective measurements are carried out for different reverse biases, so that all QD internal levels are probed. For all samples and measurements, the temperature is swept from 50 to 400 K in steps of 5 K. For conventional DLTS measurements, $V_m = 6$ V (reverse bias) and $V_p = 0$ V, whereas for charge-selective DLTS V_m is swept from 1 to 6 V (reverse bias) in 1 V steps with $V_p = V_m - 1$ V. The capacitance transients are measured at a frequency of 1 MHz and an AC voltage of 100 mV. The pulse length is chosen so that the charging process is complete at all temperatures. For the *Only-QD* sample, the pulse length is 0.2 s and the measurement time 1.8 s, while for the *Only-Barr* sample, 0.5 and 2.5 s, and for the sample *QD-Barr*, 2 and 8 s are used. The reference times τ_{ref} for all samples range between 0.5 and 5 s. The DLTS signals of the three types of samples are shown in **Figure 8**. The peak of *Only-QD* is centered around 110 K, that of sample *Only-Barr* around 230 K, while for *QD-Barr* it appears at higher temperatures: between 280 and 400 K. This suggests a larger localization energy than that of *Only-QD*, as expected from the presence of the additional AlP barrier.

The *Only-QD* sample shows the smallest activation energy: $E_a = 0.298$ (± 0.006) eV. For *Only-Barr* the activation energy represents the height of the energy barrier formed by AlP on GaP and amounts to 0.63 (± 0.01) eV, in agreement with the values reported in literature, ranging between 0.34 and 0.69 eV.[30] The E_a for *QD-Barr* is determined to be 0.86 (± 0.02) eV, which is
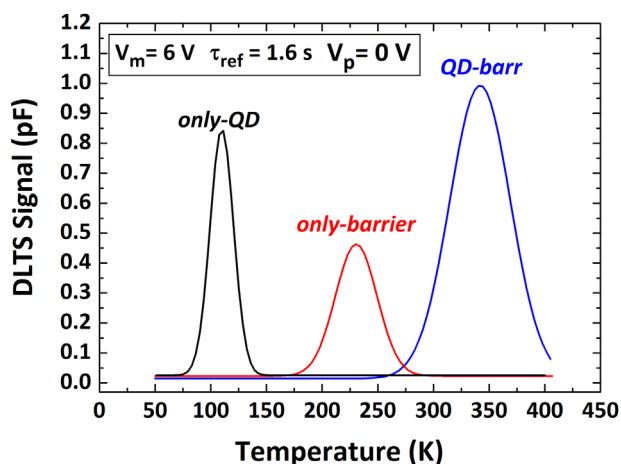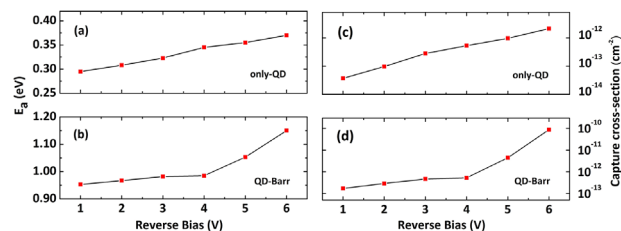
Figure 9. Capture cross-sections and activation energies extracted from the charge-selective DLTS measurements for *only-QD* (a,c) and *QD-Barr* (b,d).

consistent with the sum of the activation energies of *Only-QD* and *Only-Barr*, that is, 0.92 (± 0.01) eV. The values for the capture cross-section are as follows: $(4.6 \pm 1.2) \times 10^{-12}$, $(6.6 \pm 1.7) \times 10^{-12}$, and $(1.4 \pm 0.4) \times 10^{-14}$ cm^2, for *Only-QD*, *Only-Barr*, and *QD-Barr*, respectively.

The charge-selective DLTS measurements were performed on the *only-QDs* and the *QD-Barr* samples to determine the *hole localization energy* E_{loc} for QDs with and without AlP barrier. **Figure 9**a and b show the energies of QD levels extracted from the measurements at different voltages for both samples. The voltage $V_m = +6$ V is the largest value for which hole localization in QDs can be detected and therefore the energy value measured at this voltage represents the hole ground state in QDs. For the *only-QD* E_{loc} is determined to be 0.370 (± 0.008) eV, while for *QD-Barr* 1.15 (± 0.02) eV. It is important to point out that the 1.15 eV localization energy represents here the combined effect of the AlP barrier and the QDs. In Figure 9c and d the capture cross sections of *only-QD* and *QD-Barr* are plotted versus the reverse bias: for *only-QD*, it is determined to be $(2.1 \pm 0.5) \times 10^{-12}$ cm^2, while for *QD-Barr* is $(9 \pm 5) \times 10^{-11}$ cm^2.

Assuming GaAs incorporation to the QDs reducing the actual Sb contents in InGaSb QDs, we expect E_{loc} to lie in-between the valence band discontinuity (or valence band offset, VBO) QDs/matrix of the two heterostructures $In_{0.5}Ga_{0.5}As/GaP$ and $In_{0.5}Ga_{0.5}Sb/GaP$. The IFIGS-and-electronegativity concept is to date considered a good method for providing such an estimate. Indeed, this theory has recently been well confirmed for the material system GaSb/GaP, where the predicted VBO of 0.67 eV agrees very well with the measured value of 0.65 eV between GaSb QDs and GaP matrix.[31] For the two QD-systems $In_{0.5}Ga_{0.5}As/GaP$ and $In_{0.5}Ga_{0.5}Sb/GaP$ it yields values for VBOs of ≈ 0.3 and ≈ 0.6 eV, respectively,[32,33] and therefore the measured value of $E_{loc} = 0.370$ (± 0.008) eV is within the predicted limit. Finding a lower value for E_{loc} than the predicted ≈ 0.6 eV for $In_{0.5}Ga_{0.5}Sb/GaP$ is in agreement with significant As incorporation into QDs suggested above. The storage time τ for

Figure 8. Conventional DLTS measurements at $\tau_{ref} = 1.6$ s of the three different structures are displayed.

Table 1. Localization energies and capture cross-sections obtained by charge-selective DLTS, together with the extrapolated storage times for the two QD-samples. The errors on σ_∞ and τ are reported in orders of magnitude in brackets.

Sample	E_{loc} [eV]	σ_∞ [cm^2]	τ [s]
Only-QD	0.370 (± 0.008)	$(2.1 \pm 0.5) \times 10^{-12}$	$(7.7 \pm 1.3) \times 10^{-9}$
QD-Barr	1.15 (± 0.02)	$(9 \pm 5) \times 10^{-11}$	3200 (± 300)

holes captured in QDs at room temperature are extrapolated by using Equation (1). In **Table 1** they are listed together with the hole localization energies and capture cross-sections for the two QD-samples, alongside with their errors.

5. Storage Time

The highest τ is found for the *QD-Barr* structure, which amounts to 3200 ($\pm$300) s (almost 1 h). This result marks an improvement a factor of 14 with respect to our former result of 230 ($\pm$60) s for MOVPE-grown $In_{0.5}Ga_{0.5}As/GaP$ QDs,[6] where E_{loc} for the QDs + AlP system was determined to be 1.14 ($\pm$0.04) eV and σ_∞ to $(8 \pm 5) \times 10^{10}$ cm^2. This represents hitherto the record of hole retention time for QDs fabricated by MOVPE. The increase of τ can be solely attributed to the reduction by one order of magnitude of the capture cross-section, compared to the one of $In_{0.5}Ga_{0.5}As/GaP$ QDs QDs,[6] that is, from $(8 \pm 5) \times 10^{10}$ to $(9 \pm 5) \times 10^{11}$ cm^2, while E_{loc} for $In_{0.5}Ga_{0.5}As$ and InGaSb QDs are comparable. We ascribe this effect to the use of Sb instead of As in QDs. Further understanding of this process requires more detailed chemical analysis of the QD composition and additional theoretical modeling of capture processes. In fact, once such a method is developed, the measured localization energy E_{loc} = 1.15 eV would suffice for non-volatility, provided that the capture cross-section be reduced to $\sigma_\infty = 10^{-14}$ cm^2. Of course, non-volatility can be also achieved by using other material combinations for QDs and matrix, like $GaSb/Al_{0.51}In_{0.49}P$ QDs, where the localization energy is estimated to be $\approx$1.25 eV.[3]

6. Conclusions

We have investigated the impact of two critical MOVPE parameters, Sb-soaking and GRI, on structural, optical, and charge storage properties of nominal InGaSb/GaP QDs. Sb-soaking prior to InGaSb deposition is found to reduce QD dimensions while increasing their density. GRI increases the size of QDs through a ripening process. Both methods lead to an improvement of the overall QD optical quality. Deep-level-transient spectroscopy investigations have been carried out on such QDs to measure storage times of hole carriers captured in QD states. The maximum measured storage time (with an additional AlP barrier) is 3200 ($\pm$300) s at room temperature, with an associated capture cross-section of $(9 \pm 5) \times 10^{11}$ cm^2. The capture cross-section is found to be reduced by an order of magnitude with respect to the one of $In_{0.5}Ga_{0.5}As/GaP$ QDs grown by MOVPE demonstrating the impact of using Sb. Optical and electrical data indicate a significant diffusion of As into InGaSb. MOVPE growth processes with reduced As incorporation will be developed in the future in order to achieve even larger localization energies and longer storage times. Most important is the proof presented here, that MOVPE is a valid technology for mass production of such devices, although still some work has to be done.

Conflict of Interest

The authors declare no conflict of interest.

[1] M. Geller, A. Marent, D. Bimberg, in *Handbook of Nanophysics: Nanoelectronics and Nanophotonics* (Ed: K. D. Sattler), CRC Press, Boca Raton, FL **2010**, Sect. 2.1.

[2] A. Marent, T Nowozin, M. Geller, D Bimberg, *Semicond. Sci. Technol.* **2011**, *26*, 014026.

[3] D. Bimberg, A. Marent, T. Nowozin, A. Schliwa, *Proc. SPIE* **2011**, *7947*, 79470L.

[4] A. Marent, M. Geller, D. Bimberg, *Microelectron. J.* **2009**, *40*, 492.

[5] E. M. Sala, G. Stracke, S. Selve, T. Niermann, M. Lehmann, S. Schlichting, F. Nippert, G. Callsen, A. Strittmatter, D. Bimberg, *Appl. Phys. Lett.* **2016**, *109*, 102102.

[6] L. Bonato, E. M. Sala, G. Stracke, T. Nowozin, A. Strittmatter, M. N. Ajour, K. Daqrouq, D. Bimberg, *Appl. Phys. Lett.* **2015**, *106*, 042102.

[7] L. Bonato, I. F. Arikan, L. Desplanque, C. Coinon, X. Wallart, Y. Wang, P. Ruterana, D. Bimberg, *Phys. Status Solidi B* **2016**, *253*, 1877.

[8] P. Blood, J. W. Orton, *The Electrical Characterization of Semiconductors: Majority Carriers and Electron States*. Academic, London **1992**.

[9] T. Nowozin, A. Marent, M. Geller, D. Bimberg, N. Akcay, N. Oncan, *Appl. Phys. Lett.* **2009**, *94*, 042108.

[10] T. Nowozin, *Self-Organized Quantum Dots for Memories, Electronic Properties and Carrier Dynamics*, Springer, Berlin **2014**.

[11] T. Nowozin, D. Bimberg, K. Daqrouq, M. N. Ajour, M. Awedh, *Appl. Phys. Lett.* **2013**, *102*, 052115.

[12] V. Rideout, *Solid-State Electron.* **1975**, *18*, 541.

[13] I. Mojzes, T. Sebestyen, D. Szigethy, *Solid State Electron.* **1982**, *25*, 449.

[14] V. Malina, R. Soukupová, *Thin Solid Films* **1985**, *125*, L21.

[15] D. Guimard, M. Ishida, L. Li, M. Nishioka, Y. Tanaka, H. Sudo, T. Yamamoto, H. Kondo, M. Sugawara, Y. Arakawa, *Appl. Phys. Lett.* **2009**, *94*, 103116.

[16] A. Portavoce, I. Berbezier, A. Ronda, *Phys. Rev. B* **2004**, *69*, 155416.

[17] Y. I. Mazur, V. G. Dorogan, G. J. Salamo, G. G. Tarasov, B. L. Liang, C. J. Reyner, K. Nunna, D. L. Huffaker, *Appl. Phys. Lett.* **2012**, *100*, 033102.

[18] M. Copel, M. C. Reuter, E. Kaxiras, R. M. Tromp, *Phys. Rev. Lett.* **1989**, *63*, 6.

[19] D. Guimard, M. Nishioka, S. Tsukamoto, Y. Arakawa, *J. Cryst. Growth* **2007**, *298*, 548.

[20] D. Guimard, S. Tsukamoto, M. Nishioka, Y. Arakawa, *Appl. Phys. Lett.* **2006**, *89*, 083116.

[21] D. R. Wight, *J. Phys. C: Solid State Phys.* **1968**, *1*, 1759.

[22] F. Heinrichsdorff, A. Krost, M. Grundmann, D. Bimberg, F. Bertram, J. Christen, A. Kosogov, P. Werner, *J. Cryst. Growth* **1997**, *170*, 568.

[23] K. Pötschke, L. Müller-Kirsch, R. Heitz, R. L. Sellin, U. W. Pohl, D. Bimberg, N. Zakharov, P. Werner, *Physica E* **2004**, *21*, 606.

[24] M. A. Herman, D. Bimberg, J. Christen, *J. Appl. Phys.* **1991**, *70*, R1.

[25] J. A. Prieto, G. Armelles, M.-E. Pistol, P. Castrillo, J. P. Silveira, F. Briones, *Appl. Phys. Lett.* **1997**, *70*, 25.

[26] G. Stracke, E. M. Sala, S. Selve, T. Niermann, A. Schliwa, A. Strittmatter, D. Bimberg, *Appl. Phys. Lett.* **2014**, *104*, 123107.

[27] D. V. Lang, *J. Appl. Phys.* **1974**, *45*, 3023.

[28] S. M. Sze, K. K. Ng, *Physics of Semiconductor Devices*, 3rd ed., Wiley, New York **2006**.

[29] M. Geller, C. Kapteyn, L. Müller-Kirsch, R. Heitz, D. Bimberg, *Appl. Phys. Lett.* **2003**, *82*, 2706.

[30] I. Vurgaftman, J. R. Meyer, *J. Appl. Phys.* **2001**, *89*, 5815.

[31] L. Desplanque, C. Coinon, D. Troadec, P. Ruterana, G. Patriarche, L. Bonato, D. Bimberg, X. Wallart, *Nanotechnology* **2017**, *28*, 225601.

[32] W. Mönch, *Mater. Sci. Semicond. Process.* **2014**, *28*, 2.

[33] W. Mönch, *Electronic Properties of Semiconductor Interfaces*, Springer, Berlin **2004**, Sec. 5.6 and 6.2.

1800182 (7 of 7)